Chromium Oxide-Ruthenium Oxide Solid Solution Anode Implemented in a Solid Phosphate Electrolyzer at 240 °C and 28 Bar Overpressure

Bannert, F.; Christensen, E.; Berg, R. W.; Köhler, K.; Bjerrum, N. J.

Published in:
Journal of the Electrochemical Society

Link to article, DOI:
10.1149/1945-7111/ad2055

Publication date:
2024

Document Version
Publisher's PDF, also known as Version of record

Journal of The Electrochemical Society, 2024 **171** 013505

Chromium Oxide-Ruthenium Oxide Solid Solution Anode Implemented in a Solid Phosphate Electrolyzer at 240 °C and 28 Bar Overpressure

F. Bannert,[1,*] E. Christensen,[2] R. W. Berg,[3] K. Köhler,[1] and N. J. Bjerrum[2,,z]**

[1]*Department of Chemistry, Catalysis Research Center, Technical University of Munich, D-85748 Garching, Germany*
[2]*DTU Energy, Technical University of Denmark, DK-2800 Kgs. Lyngby, Denmark*
[3]*Department of Chemistry, Technical University of Denmark, Lyngby DK-2800, Denmark*

This work offers an overview of the synthesis and implementation of various chromium-ruthenium oxide materials for gas-phase solid-acid water electrolysis under hydrothermal conditions (240 °C, 28 bar of Ar and steam overpressure). The oxidic solid solutions show general stability over a broad chromium concentration range in the RuO_2 rutile structure during synthesis. Decomposition of the solid solutions is observed over a potential of around 2.1 V during electrolysis (including the Ohmic contribution of the setup and cell). Electrolysis performed below this decomposition potential shows promising results for replacing pure RuO_2 with a low ruthenium-containing anode. Special attention has been given to $Cr_{0.6}Ru_{0.4}O_2$ for being less expensive because of the lower ruthenium content and showing good stability and comparable performance to RuO_2 during continuous chronopotentiometry operation for 1 h at 75 mA cm^{-2} current densities.
 [DOI: 10.1149/1945-7111/ad2055]

Manuscript submitted September 19, 2023; revised manuscript received January 5, 2024. Published January 30, 2024.

Supplementary material for this article is available online

In order to reduce the anthropogenic greenhouse gas emissions that lead to climate changes, the European Union has committed itself as part of the Green Deal to achieving climate neutrality by the year 2050 through targeted decarbonization.[1]

Among other things, successes have already been achieved by implementing regenerative energy sources, e.g., through wind power. However, compared to conventional power plants, these sources do not offer a steady flow of energy and can lead to both undersupply and oversupply in the electrical grid. At the same time, electrical energy storage represents a costly technical challenge.[2]

With the aim of covering energy production fluctuations and reducing the emission of CO_2, it is now clear that it is necessary to convert CO_2 into new fuels by using electricity from green sources. This method is based on the idea that carbon dioxide can be viewed as another carbon source that can be used to produce chemicals, e.g., hydrocarbons, for energy storage and even as a value feedstock for producing high-quality chemical materials as an alternative to petrochemicals. This can be done by first producing hydrogen by electrolysis of water and then using the produced hydrogen to let it react with CO_2 to form new fuels and chemicals. In a similar way, we presented an approach that specialized in implementing a one-step process, i.e., the production of, e.g., CH_4 or CH_3OH from H_2O, CO_2, and electricity in one reactor.[3–9]

However, no matter the approach, oxygen is produced at the anode leading to material stability issues. In particular, reducing the overpotential on the anode represents a difficult challenge. In the case of acidic electrolytes, IrO_2 and RuO_2 have shown superior catalytic properties. However, of these, only IrO_2 shows sufficient chemical stability for prolonged use. On the other hand, RuO_2 has the highest activity.[10–16] Unfortunately, iridium is very rare and increasingly expensive. At the same time, the price of ruthenium has also increased considerably. This trend in economic unavailability for both widely implemented metal oxides motivates the research for supplementary anode materials.[17]

The reason for the limited stability of RuO_2 during oxygen evolution reaction (OER) is believed to depend on Ru(VI) species formed during the oxidation reaction, which determine if the catalytic OER cycle intermediate RuO_4 is lost into the solution or the gas phase.[18] This accounts for PEM cells where liquid water is constantly flowing across the anode. If the conditions are changed to gas phase electrolysis and temperatures above 200 °C as it is in the present case it might be different: There will be no liquid phase to dissolve anything. In addition, the RuO_4 will decompose very fast. RuO_4 is not thermodynamic stable even at room temperature but it decompose very slowly with a half-life of 8.9×10^5 h at 25 °C.[19] On the contrary the half-life at 240 °C is 0.0001 h (extrapolated value[19]).

On this basis, we found it relevant to test RuO_2 electrode materials in our previously reported intermediate temperature steam electrolysis setup.[5,8,9] However, as already mentioned, the price of ruthenium is high and going up, and therefore there is a necessity to keep the implemented amount as low as possible.

An interesting approach with regards to this is given by the implementation of low-ruthenium content oxides by Lin et al.[20] in which they very recently showed that a solid solution of CrO_2 in RuO_2 with a rutile structure and a $Cr_{0.6}Ru_{0.4}O_2$ composition can be used as an anode in 0.5 M H_2SO_4 with a low overpotential of only 178 mV at a current density of 10 mA cm^{-2}. Their results serve as a starting point and motivation for our contribution, that shows a technical-oriented/pragmatic implementation of the chromium-ruthenium oxides as anode materials.

In the subsequent sections, we present a synthesis method with simple inorganic precursors and preparation steps for chromium ruthenium solid solution oxides, characterize them, and demonstrate their implementation as less expensive anode material substitutes to RuO_2 in a medium-temperature pressurized solid phosphate electrolyzer.

Experimental

Preparation of the electrolyte.—The proton conducting electrolyte CsH_2PO_4 (CDP, CAS no. 69089–35–6) was prepared as described in previous publications[4,8,9] by dissolution of 375 g caesium carbonate (99%, Reagent Plus, CAS no. 534–17–8) in 600 ml deionized water and subsequent mixed with 265 g concentrated phosphoric acid (85 wt%, CAS no. 7664–38–2) for obtaining a Cs to P mol ratio of 1:1. The mixture was stirred at room temperature for at least 4 h. Afterward, 750 ml of methanol (Puriss p.a., ACS reagent, CAS no. 67–56–1) were slowly added to precipitate the CDP. Thereafter the CDP was isolated by filtration,

*Electrochemical Society Student Member.
**Electrochemical Society Member.
[z]E-mail: nibj@dtu.dk

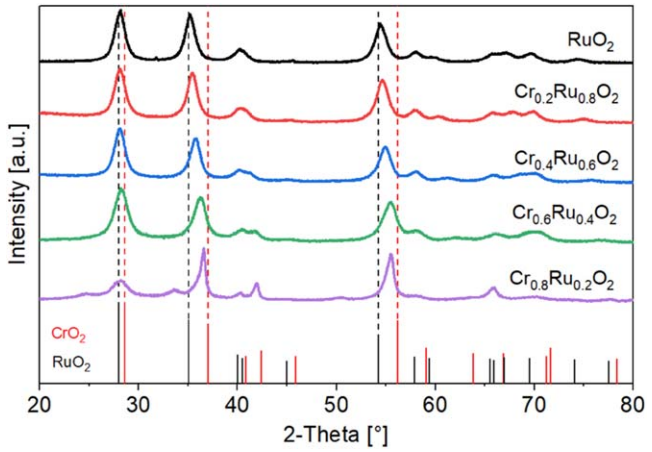

Figure 1. PXRD patterns for the synthesized ruthenium oxide and chromium-ruthenium oxides up to 0.8 chrome fraction. The (110), (101), and (211) crystalline planes of RuO_2 and CrO_2 are demarked with vertical dashed lines against reference stick patterns visualizing the rutile structure reflex shifts[23,24].

subsequently washed with methanol to remove any remaining phosphoric acid, and then dried overnight at 90 °C. Finally, the CDP was dissolved in water and recrystallized.

Preparation of the proton-conducting membrane.—We then applied proton-conducting membranes consisting of a mixture of CDP with polyvinyl butyral (PVB) that have been prepared and also characterized as described in previous publications.[8,9] The membrane casting was done by the Danish company Blue World Technologies ApS. For the casting, the CDP was ball milled and mixed with a solution of PVB in propan-2-ol to form a slurry. The slurry was casted to a thickness of approximately 0.6 mm and left to dry.

The casted electrolyte was then cut into circular disks with a diameter of around 42 mm, layered in-between two Teflon discs (0.5 mm thickness), and at 160 °C pressed with a pressure of 144 kg cm^{-2} for 45 min. After cooling, the electrolyte thickness was about 0.35 mm.

Preparation of the electrodes.—The electrodes consist of double-layered steel (316 L) felts with 8 and 12 μm fiber diameters acting as gas diffusion layers; the finer fibers are placed towards the electrolyte membrane. All electrodes have a thickness of around 0.5 mm. The electro-coating of the electrodes was performed by the Danish company Elplatek A/S. First, a Ni strike layer is deposited by electroplating, followed by a Pt layer for the cathode or a Miralloy (Cu-Sn-Zn) layer followed by a Ru layer for the anode. Since the condition on the anode side is rather harsh the Ru layer is routinely checked with SEM-EDX before the experiments.

Synthesis of chromium-ruthenium oxide solid solutions.—The solid solutions that were applied as electrocatalysts were synthesized from chromium(III)-nitrate-nonahydrate (pure) from Riedel-de Haën and ruthenium(III) nitrosyl nitrate (crystalline, Ru 31.3% min) from Alfa Aesar. These compounds were weighed in amounts corresponding to ca. 3.00 g of the final solid solution of CrO_2 in RuO_2 or the pure compounds. The material was then dissolved in ca. 75 ml distilled water in a beaker placed on a heating plate. After this, the water was evaporated and the material decomposed by heating the plate for some time at 200 °C and later at 310 °C. During this procedure, yellow to brown vapors appeared above the dried salts. After a while, the vapor disappeared, and it was possible with a glass spatula to crush the material into a powder. After this, the salt was heated in air for 4 h at 550 °C. By this procedure the material further decomposed into a fine powder. Finally, the powder was ground in an agate mortar for ca. 5 min. As shown later, this procedure resulted in a homogeneous product even at relatively low ruthenium contents.

Ink preparation and application of solid solutions onto the anode-.—Electrocatalyst inks were prepared by mixing together in a vial 5 g formic acid (98–100 wt%, CAS no. 64–18–6), 1 g of a solution with 0.5 wt% polybenzimidazole (PBI, Celanese Corp.) in formic acid, and 0.6 mmol of the solid solution. This suspension was placed in an ultrasonic bath for 2 h before application with a spray gun on a 150 °C pre-heated (Ru-coated) anode.

The main effort was to compare different solid solutions. No trial to understand the system as such was undertaken (e.g. utilization of the catalyst and the contact between catalyst and the separator). We decided that everything was in order when the resistance was measured and found of the right size.

Besides always using 0.6 mmol of the solid solution the following procedure was followed: Ink coverage on the anode felts was mainly on the uppermost fiber layer, which was covered entirely without affecting the porosity of the electrode. This uppermost layer is effectively in contact with the electrolyte membrane when the cell is assembled. See light microscopy images of a general example of the anodes before and after ink application in the Supplemental Material Fig. S1.

Measurements of electrical conductivity of chromium-ruthenium oxide solid solutions.—The next step was to measure the specific conductivity of the solid solution powders. It proved to be a more difficult task than expected. The measurements were performed in a custom-made holder with two pistons with a diameter of 12.60 mm enclosed in a plastic cylinder. The holder was equipped with a micrometer clock so that the thickness of the sample could be measured with a precision of 0.01 mm. The electrical 4-point measurements were performed with an ILOM-508A MILLIOHM METER, with an accuracy of 0.1 mOhm, and with a KEITHLEY 580 MICRO-OHM METER, with a precision of 0.01 mOhm. The measured amounts of the oxides were in the range of ca. 0.40 g ($Cr_{0.8}Ru_{0.2}O_2$) to 1.00 g (RuO_2) for obtaining a ca. 2.5 mm thickness at an external pressure of 40 kg force (kgf) cm^{-2}. It is well known that at larger thickness of the samples, there is no proportionality between resistance and thickness of the sample since the sample sticks to the sideway of the cylinder.[21]

Notably, the measurements showed significant variation due to how the powders could orient themselves during pressing. In order to address this observation, the following procedure was performed on all the samples to allow a uniform testing procedure with more reproducible results: After the cylinder was filled with the weighed material and the upper piston was placed in the cylinder, the cylinder was turned completely clockwise six times, and the same procedure was then performed counter-clockwise and so on altogether six times.

Electrolysis setup and experimental conditions-.—The electrolyzer has an electrode-membrane-electrode construction between two current collector plates with gas-flow patterns. Electrically insulating polyimide (Kapton, DuPont de Nemours Inc.) and gas-sealing soft graphite paper (Papyex, Mersen S.A.) layers are implemented as the gasket material. For a detailed description of the electrolysis cell, the electrolyzer setup, and further information on the super-protonic properties of the electrolyte under experimental conditions, we refer to the original apparatus patent [3] and previous publications.[5,8]

The electrolysis cell is heated up to 240 °C under a constant flow of around 50 ml min^{-1} of Ar at an overpressure of 28 bar on both the cathode and the anode side. A water vapor partial pressure of approximately 6.8 bar is constantly maintained on both gas streams throughout the experiments. Electrochemical measurements and characterizations were performed with a two-terminal connection on a VersaStat 4 potentiostat from Princeton Applied Research. For cell conditioning at the beginning of each experiment,

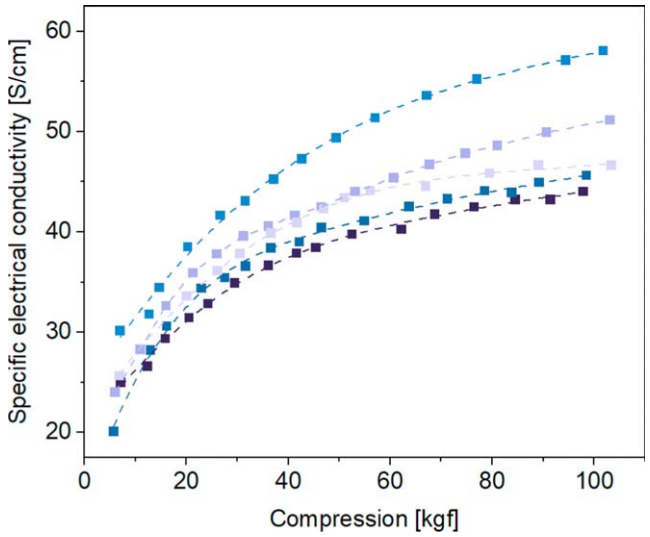

Figure 2. Specific electrical conductivity of synthesized *pure* RuO_2 powders as a function of compression. Weight of each sample ca. 1.00 g. Area of sample 1.247 cm^2.

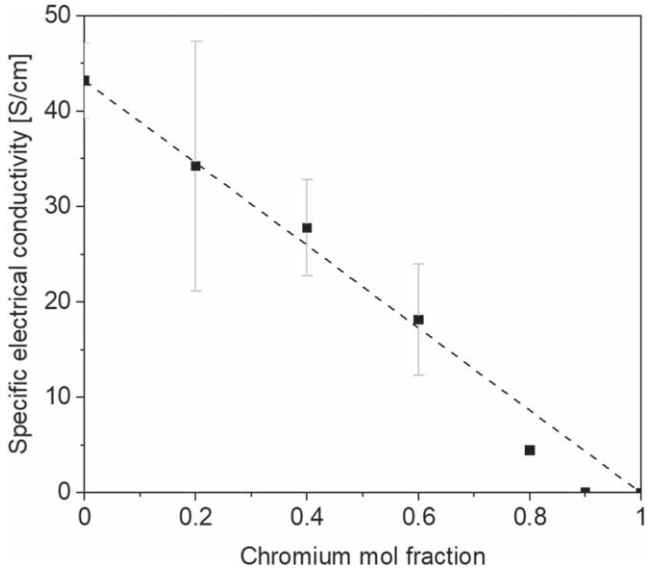

Figure 3. The specific electrical conductivity for the synthesized $Cr_{0.x}Ru_{1-0.x}O_2$ powders at a pressure of 40 kgf cm^{-2} with standard error bars. Chromium mole fraction 1 is pure Cr_2O_3 and not CrO_2.

chronopotentiometry at 30 mA cm^{-2} was performed for 5 min until the potential was stable.

Results and Discussion

Characterization of chromium-ruthenium oxides.—The synthesis method with the implementation of inorganic salt precursors presented in this contribution leads to the formation of the desired chromium-ruthenium solid solutions, in contrast to other more complex methods implemented in literature, e.g., using specialized precursors like chromium MOFs;[20] or special preparation steps like the reduction of potassium dichromate solutions and their controlled precitipation.[22]

Powder X-ray diffraction (PXRD) patterns for the prepared chromium-ruthenium oxides were comparable to those of Lin et al.[20] and showed the formation of a solid solution between chromium and ruthenium with a characteristic rutile structure attributed to the Ru(IV) and Cr(IV) oxides, see Fig. 1. In contrast to us, Lin et al. only characterized and tested chromium mol fractions at 0.60 and higher.

With increasing Cr content, a reflex shift toward higher 2-Theta angles was observed, especially for the (101) and (211) rutile structure planes in accordance with expected decreasing crystal unit cell lattices. These observations speak for the formation of an oxide solid solution between chromium and ruthenium.[22] Furthermore, the absence of perceivable ferromagnetism in the prepared oxides, expected to come from CrO_2, indicates a homogeneous/uniform dispersion of both Cr and Ru due to possible dilution effects inside the crystalline rutile structure. Additional determination of the solid solution composition and dispersion by elemental X-ray mapping (EDS) confirms the homogeneous distribution of the elements in the samples; for a representative $Cr_{0.6}Ru_{0.4}O_2$ sample SEM image and X-ray maps of chromium and ruthenium see Supplemental Material Fig. S2.

The thermodynamically metastable Cr(IV) species seems to be stabilized by the matrix effects of the thermodynamically stable RuO_2 rutile structure even after the high calcination temperatures and prolonged times implemented during the synthesis (up to 550 °C, air, 4 h). This observation supports a strong RuO_2 matrix stabilizing effect for the Cr(IV) oxidation state in the solid solution, that is observed even at high chromium concentrations (higher than 0.5) still showing good PXRD-crystallinity for the rutile structure and (up to 0.8 chromium) the absence of other chromium phases with different oxidation states, e.g., chromium(III) oxide (not detected by the PXRD method). With a mol fraction of about 0.8 chromium and higher, a heterogeneous Cr_2O_3 phase is present, denoted by its characteristic corundum crystalline structure (Supplemental Material Fig. S3 for additional patterns showing the appearance of this phase). This observation is in accordance with Lin et al.,[20] who also showed the presence of Cr_2O_3 at chromium mol fraction concentrations of around 0.7 and higher.

This does not imply that a solid solution between Cr(IV) and Ru (IV) oxides is concentration-limited, since a linear substitution and mixing between the rutile structure phases of RuO_2 and CrO_2 should be ideally possible. The appearance of the corundum structure from Cr_2O_3 only denotes the concentration stabilizing limit of the RuO_2 rutile structure under the given synthesis conditions.

As mentioned in the experimental section, the conductivity of the same sample varied considerably between measurements, possibly due to the different packing of the oxide particles in each experiment. This is exemplified in Fig. 2 with some conductivity measurements of the prepared RuO_2 powder against compression.

Similar patterns were found for the various solid solution compositions, some with more variation in the measurements and some with less.

Figure 3 shows the final results of the electrical conductivity measurements of the different pure and mixed oxides formed from the synthesis method and conditions described in the experimental section. Note that the sample with a chromium mol fraction of 1 is Cr_2O_3 and not CrO_2. The shown values are the average of 5 measurements except for pure Cr_2O_3 and $Cr_{0.9}Ru_{0.1}O_2$, where only two measurements for each composition have been made.

Despite the spread in the measurements, the most obvious explanation is a linear decreasing trend in conductivity with decreasing ruthenium content aimed at zero conductivity for the formed Cr_2O_3 when there is no ruthenium present (compared with the dashed line). It is expected that CrO_2 does not contribute much to the conductivity of the mixed oxides since the electrical conductivity of CrO_2 is quite a bit lower than the conductivity of RuO_2. For instance, Kubota et al.[25] report a value for compressed CrO_2 powder of 4.3 S cm^{-1} at 75 kgf cm^{-2}. This should be compared with our average value of 49.0 S cm^{-1} for RuO_2, also at 75 kgf cm^{-2} (we have, however, found no literature value to directly compare with our RuO_2 powder).

As expected, the conductivity at higher chromium content will decrease further due to the appearance of Cr_2O_3 heterogeneous phases. At a mol fraction of around 0.90, the conductivity is already

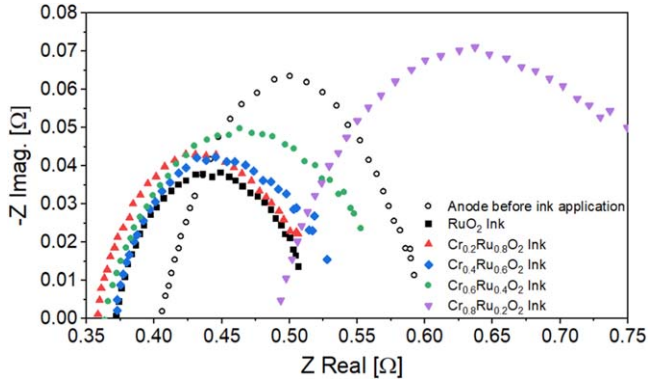

Figure 4. Potentiostatic EIS measurements at 1.7 V with a frequency range from 1 MHz to 1 Hz for the electrochemical cell at 240 °C under 28 bar overpressure of argon with steam supplied to both the anode (varying systems) and cathode (Pt-coated steel felt) with CDP/PVB electrolyte membranes.

Table I. Specific cell resistance for all tested samples. Each value was determined from EIS, membrane thickness, and electrode area.

Sample	Specific cell resistance [Ωm]
Anode before application	0.88
All samples RuO_2 to $Cr_{0.6}Ru_{0.4}O_2$	0.77
$Cr_{0.8}Ru_{0.2}O_2$	1.11

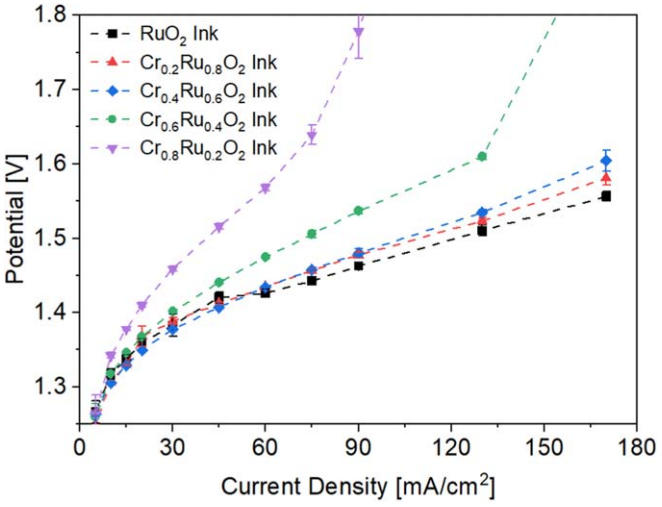

Figure 5. Polarization curves for electrolysis cells at 240 °C under 28 bar overpressure of argon with steam supplied to both the anode (varying systems) and cathode (Pt-coated steel felt) with CDP/PVB electrolyte membranes. The potential is adjusted to exclude the Ohmic contribution from the electrolyte and equipment.

very low, and it is close to zero at pure Cr_2O_3. An important question here is, of course, how the conductivity relates to the "activity" of the material. As presented later, the overpotential of the oxides increases with increasing chromium content and correlates to the conductivity decrease shown in Fig. 3. It should be taken into account that the electrical conductivity of RuO_2 decreases with increasing temperature. According to the measurements of Ryden and Lawson[26] the decrease in conductivity of a single crystal of RuO_2 in going from 25 °C to 240 °C is 45%.

Electrolysis performance of chromium-ruthenium oxides as anode materials.—The central motivation of this work lies in the study of the electrocatalytic behavior of the chromium-ruthenium oxides and the related possibility of implementation and durability of inexpensive materials that show good electrocatalytic properties and stability. A main reference work for this experimental series is represented by the studies from Lin et al.[20] that showed promising properties of the Cr/Ru solid solution, especially the $Cr_{0.6}Ru_{0.4}O_2$ oxide when applied for the oxygen evolution reaction in an aqueous acid electrolyte system. Thus, the following implementation of the Cr/Ru solid solutions in our analogous solid-acid gas-phase electrolyzer will evaluate the application of these materials at a technical level system and give more insights into their economic scalability possibilities.

Within this framework, electrochemical impedance measurements (EIS) were taken for the solid solutions with varying chromium-to-ruthenium ratios. The solid solutions showed an overall polarization and cell resistance improvement compared to the Ru-coated anode with no ink, see Fig. 4. The polarization resistance increases with an increment in the Cr content. The worst-performing solid solutions were the sample with the highest chromium content ($Cr_{0.8}Ru_{0.2}O_2$), which showed the lowest specific electrical conductivity, Fig. 3, and the sample with the presence of non-conducting Cr_2O_3 characteristic corundum structure reflexes in the PXRD, see Fig. 1.

The specific cell resistances of the applied inks, except for $Cr_{0.8}Ru_{0.2}O_2$, had all the same value laying lower than the resistance of the Ru-coated electrode with no ink, see Table I.

Similarly, the observations from Fig. 4 are reflected in the electrolysis performance of the solid solutions, see Fig. 5. The polarization curves were obtained by step chronopotentiometry measurements at different current densities. The error bars show the maximum deviation observed over at least 120 s for each point. Note that the RuO_2 measurement at 45 mA cm^{-2} is an outlier from the polarization curve, but the error bar places that single measurement point in the expected range.

The solid solutions with chromium mole fractions up to 0.4 show comparable water electrolysis performance to RuO_2 in ranges up to 170 mA cm^{-2}. These promising results speak for the implementation of Cr/Ru solid solutions instead of pure RuO_2. At the same time, the advantageous performance of the solid solutions decreases with increasing Cr content. This correlates with the measured conductivity decrease dependent on the increasing chromium content.

Furthermore, a slope change was observed for high chromium content anodes above the adjusted potential of around 1.7 V (excluding the ohmic contribution of the cell and setup), especially for samples with a chromium mol fraction of 0.6 or higher. Notably, the solid solutions show degradation above a specific potential, leading to stability boundaries that limit the practical implementation possibilities. To address the observed solid solution instability phenomenon, constant chronoamperometry at a value slightly above the decomposition potential (2.2 V without excluding the Ohmic contribution of the setup and cell) was performed to control the anode's degradation. Post-mortem leaching studies of the anodes were done following the procedure: the anode was taken out of each cell and placed inside a vial with deionized water. Immediately, a yellow coloring of the solution was observed and confirmed with UV–vis spectroscopy to be coming from hexavalent chromates in the solution. For this, a reference potassium chromate K_2CrO_4 solution was used. Leaching samples were prepared to pH 12 with aqueous potassium hydroxide to allow the predominant speciation of CrO_4^{2-} for a better comparison to the reference and literature spectroscopy values.[27] Both the reference and the leaching sample showed characteristic chromate transmission bands from CrO_4^{2-} in the ultraviolet spectral range at around 230 nm and 312 nm;[28,29] see Supplemental Material Fig. S4 for the UV–vis Spectra. Note that the anodes did not show any coloration if the leaching test was performed before electrolysis.

The chromium leaching out of the solid solution anodes after degradation proves the presence of Cr(VI) species, more specifically, chromates(VI), that can only come from the oxidation of the

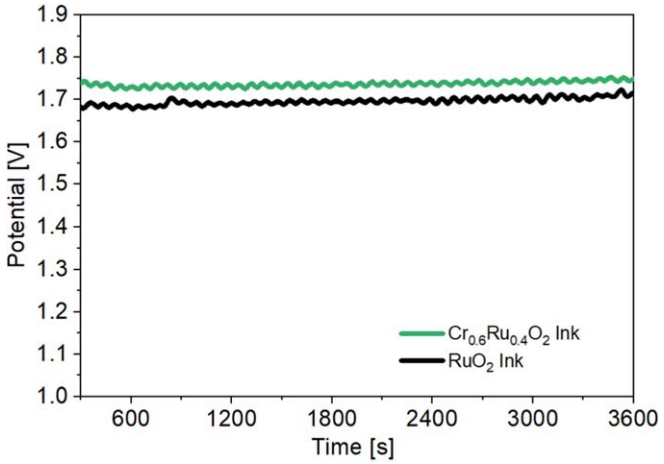

Figure 6. Chronopotentiometric measurements at 75 mA cm^{-2} comparing the $Cr_{0.6}Ru_{0.4}O_2$ solid solution to the pure RuO_2 system for a period of 1 h at 240 °C under 28 bar overpressure of argon with steam supplied to both the anode (varying systems), cathode (Pt-coated steel felt) with CDP/PVB electrolyte membrane. The Ohmic contribution of the setup and cell is not excluded.

chromium(IV) inside the solid solution due to the high oxidative potential at the anode. The stabilizing matrix effects expected from the Ru(IV) rutile structure could not keep the thermodynamically metastable Cr(IV) compound from being oxidized by the formed oxygen. This would lead to the formation of a chromium trioxide phase, affecting the conductivity and explaining the observed increase in the polarization curve slope and potential degradation. Pure CrO_3 is stable up to 250 °C[30] and is therefore expected to be stable at the present conditions.

Nevertheless, even though the solid solutions show instability after reaching a particular potential, high current densities could be implemented under the setup's harsh hydrothermal conditions within the stability range for prolonged periods of time, see Fig. 6 comparing RuO_2 to $Cr_{0.6}Ru_{0.4}O_2$. The observed potentials show a cyclic variation, of around 15 mV every 30 s between maxima, that remains over a median potential. These fluctuations are most likely caused by variations in the water vapor partial pressure coming from the evaporator. The $Cr_{0.6}Ru_{0.4}O_2$ cell had practically no performance loss (of around 12 mV) at the end of the chronopotentiometry electrolysis after 1 h.

As long as the potential remained below the solid solution decomposition threshold (at around 2.1 V, without excluding the Ohmic contribution of the setup and cell), the $Cr_{0.6}Ru_{0.4}O_2$ cell showed good performance and comparable stability to RuO_2 at 75 mA cm^{-2}, that is 530 mA total current constantly flowing through the cell, over a prolonged continuous operation of 1 h. Hence, implementing the solid solution within its stability region could be a practical, economical anode material substitute for pure RuO_2 under the harsh conditions of the technically-oriented gas-phase solid phosphate electrolyzer setup.

Conclusions

This work presented an easily applicable yet effective approach for synthesizing chromium-ruthenium solid solution oxides with rutile structure, for their implementation as anode materials. As expected, the Cr/Ru solid solutions show crystal lattice parameter decrease along with the increasing chromium content. Furthermore, the appearance of a heterogeneous Cr_2O_3 phase and a decreasing conductivity was also observed with increasing chromium content. In particular, the oxides were investigated as anode materials for water electrolysis in a gas-phase solid phosphate electrolyzer at 240 °C and a 28 bar overpressure of Ar and steam. The chromium ruthenium oxides show relatively good performance (compared to pure RuO_2). The performance decreases with increasing chromium content. Notably, the decomposition of the solid solutions, together with a substantial performance loss, was observed due to the oxidation of the metastable chromium(IV) to chromium(VI) oxide when subjected above a specific potential.

Nevertheless, if implemented below the threshold potential, the mixed oxides show good stability compared to RuO_2, allowing an application and partial substitution of the expensive ruthenium as an anode material, giving an economic advantage.

Acknowledgments

This work was supported by Innovation Fund Denmark, project file numbers 9090–00008B and INNO-CCUS 4-P1, and by the German Federal Ministry for Digital and Transport as part of the Funding Programme Renewable Fuels, project file number 16RK14005A.

ORCID

N. J. Bjerrum https://orcid.org/0000-0001-7241-4091

References

1. The European Green Deal, *COM(2019) 640* (2019), final.
2. B. Olfe-Kräutlein, H. Naims, T. Bruhn, and A. M. Lorente Lafuente, *IASS Study* (Institute for Advanced Sustainability Studies (IASS), Potsdam) (2016).
3. N. J. Bjerrum, E. Christensen, I. M. Petrouchina, A. Nikiforov, and R. W. Berg, *Patent No.*, WO2019048016 (2019).
4. A. V. Nikiforov, R. W. Berg, and N. J. Bjerrum, *Ionics*, **24**, 2761 (2018).
5. E. Christensen, I. M. Petrushina, A. V. Nikiforov, R. W. Berg, and N. J. Bjerrum, *J. Electrochem. Soc.*, **167**, 044511 (2020).
6. R. W. Berg, A. V. Nikiforov, and N. J. Bjerrum, *J. Phys. Chem. Solids*, **136**, 109177 (2020).
7. A. V. Nikiforov, I. M. Petrushina, E. Christensen, R. W. Berg, and N. J. Bjerrum, *Renewable Energy*, **145**, 508 (2020).
8. P. Bretzler, E. Christensen, R. W. Berg, and N. J. Bjerrum, *Ionics*, **28**, 3421 (2022).
9. E. Christensen, R. W. Berg, R. Krüger, and N. J. Bjerrum, *J. Electrochem. Soc.*, **170**, 014502 (2023).
10. R. R. Rao et al., *Energy Environ. Sci.*, **10**, 2626 (2017).
11. R. Kötz, H. J. Lewerenz, and S. Stucki, *J. Electrochem. Soc.*, **130**, 825 (1983).
12. S. Trasatti, *Electrochim. Acta*, **29**, 1503 (1984).
13. A. Marshall, S. Sunde, M. Tsypkin, and R. Tunold, *Int. J. Hydrogen Energy*, **32**, 2320 (2007).
14. A. T. Marshall and R. G. Haverkamp, *Electrochim. Acta*, **55**, 1978 (2010).
15. J. Cheng, H. Zhang, G. Chen, and Y. Zhang, *Electrochim. Acta*, **54**, 6250 (2009).
16. L.-E. Owe, M. Tsypkin, K. S. Wallwork, R. G. Haverkamp, and S. Sunde, *Electrochim. Acta*, **70**, 158 (2012).
17. N. T. Suen, S. F. Hung, Q. Quan, N. Zhang, Y. J. Xu, and H. M. Chen, *Chem. Soc. Rev.*, **46**, 337 (2017).
18. E. Fabri, A. Habereder, K. Waltar, R. Kötz, and T. Schmidt, *Catal. Sci. Technol.*, **4**, 3800 (2014).
19. C. Mun, L. Cantrel, and C. Madic, *Nucl. Technol.*, **156**, 332 (2006).
20. Y. Lin, Z. Tian, L. Zhang, J. Ma, Z. Jiang, B. J. Deibert, R. Ge, and L. Chen, *Nat. Commun.*, **10**, 162 (2019).
21. A. Celzard, J. F. Marêché, F. Payot, and G. Furdin, *Carbon*, **40**, 2801 (2002).
22. Y. U. Jeong and A. Manthiram, *Electrochem. Solid-State Lett.*, **3**, 205 (2000).
23. S. Gates-Rector and T. Blanton, "The powder diffraction file: a quality materials characterization database." (2004), PDF-2.
24. B. J. Thamer, R. M. Douglass, and E. Staritzky, *J. Am. Chem. Soc.*, **79**, 547 (1957).
25. B. Kubota and E. Hirota, *J. Phys. Soc. Jpn.*, **16**, 345 (1961).
26. W. D. Ryden and A. W. Lawson, *Phys. Rev. B*, **1**, 1494 (1970).
27. A. Sanchez-Hachair and A. Hofmann, *C.R. Chim.*, **21**, 890 (2018).
28. G. W. Haupt, *J. Opt. Soc. Am.*, **42**, 441 (1952).
29. M.-C. Fournier-Salaün and P. Salaün, *Open Chemistry*, **5**, 1084 (2007).
30. R. S. Schwartz, I. Fankuchen, and R. Ward, *J. Am. Chem.Soc.*, **74**, 1676 (1952).